

Rewiring with Positional Encodings for Graph Neural Networks

Rickard Brüel-Gabrielsson^{1,2} Mikhail Yurochkin^{2,3} Justin Solomon^{1,2}

Abstract

Several recent works use positional encodings to extend the receptive fields of graph neural network (GNN) layers equipped with attention mechanisms. These techniques, however, extend receptive fields to the complete graph, at substantial computational cost and risking a change in the inductive biases of conventional GNNs, or require complex architecture adjustments. As a conservative alternative, we use positional encodings to expand receptive fields to any r -ring. Our method augments the input graph with additional nodes/edges and uses positional encodings as node and/or edge features. Thus, it is compatible with many existing GNN architectures. We also provide examples of positional encodings that are non-invasive, i.e., there is a one-to-one map between the original and the modified graphs. Our experiments demonstrate that extending receptive fields via positional encodings and a virtual fully-connected node significantly improves GNN performance and alleviates over-squashing using small r . We obtain improvements across models, showing state-of-the-art performance even using older architectures than recent Transformer models adapted to graphs.

1. Introduction

Graph neural network (GNN) layers typically embed each node of a graph as a function of its neighbors' (1-ring's) embeddings from the previous layer; that is, the *receptive field* of each node is its 1-ring. Hence, at least r stacked GNN layers are needed for nodes to get information about their r -rings. Barceló et al. (2020) and Alon and Yahav (2021) identify two broad limitations associated with this structure: *under-reaching* occurs when the number of layers is insufficient to communicate information between distant vertices, while *over-squashing* occurs when certain edges act as bottlenecks for information flow.

¹Massachusetts Institute of Technology ²MIT-IBM Watson AI Lab ³IBM Research. Correspondence to: Rickard Brüel-Gabrielsson <brg@mit.edu>.

Inspired by the success of the Transformer model in natural language processing (Vaswani et al., 2017), recent methods expand node receptive fields to the whole graph (Dwivedi and Bresson, 2021; Ying et al., 2021). Since they effectively replace the topology of the graph with that of a complete graph, these works propose assorted *positional encodings* that communicate the connectivity of the input graph as node or edge features. As these methods operate on fully-connected graphs, the computational cost of each layer is quadratic in the number of nodes, obliterating the sparsity afforded by conventional 1-ring based architectures. Moreover, the success of the 1-ring GNNs suggests that local feature aggregation is a useful inductive bias, which has to be learned when the receptive field is the whole graph, leading to slow and sensitive training.

In this paper, we expand receptive fields from 1-rings to r -rings, where r ranges from 1 (typical GNN architecture) to R , the diameter of the graph (fully-connected architecture). That is, we augment a graph with edges between each node and all others within distance r in the input topology. We show that performance can be significantly improved using fairly small r and carefully-chosen positional encodings annotating this augmented graph.

Contributions. We propose applying GNN architectures to augmented graphs connecting vertices to their peers of distance $\leq r$. Our contributions are as follows:

- We increase receptive fields using a modified graph with positional encodings as edge and node features.
- We propose and compare r -ring positional encodings on the augmented graph, e.g. using spectral computations and powers of the graph adjacency matrix.
- We demonstrate that relatively small r -rings sufficiently increase performance and indeed that performance degrades in the fully-connected setting.

On our modified graphs, the top-performing GatedGCN often performs just as well as a Transformer.

2. Related Work

The Transformer model has permeated deep learning (Vaswani et al., 2017), with state-of-the-art performance in NLP (Devlin et al., 2018), vision (Parmar et al., 2018), and genomics (Zaheer et al., 2020). Its core components in-

clude multi-head attention, an expanded receptive field, positional encodings, and a CLS-token (virtual global source and sink nodes). Several works adapt these constructions to GNNs. For example, the Graph Attention Network (GAT) performs attention over the neighborhood of each node, but does not generalize multi-head attention using positional encodings (Veličković et al., 2018). Recent works use Laplacian spectra, node degrees, and shortest-path lengths as positional encodings to expand attention to all nodes (Kreuzer et al., 2021; Dwivedi and Bresson, 2021; Rong et al., 2020; Ying et al., 2021). Several works also adapt attention mechanisms to GNNs (Yun et al., 2019; Cai and Lam, 2019; Hu et al., 2020; Baek et al., 2021; Veličković et al., 2018; Wang et al., 2021b; Zhang et al., 2020; Shi et al., 2021).

Path and distance information has been incorporated into GNNs more generally. Most pertinent to our work, Yang et al. (2019) introduce the Shortest Path Graph Attention Network (SPAGAN), whose layers incorporate path-based attention via shortest paths between a center node and distant neighbors. SPAGAN uses an involved hierarchical path aggregation method to aggregate a feature for each node. Like us, SPAGAN introduces the k -ring around the center node as a hyperparameter; their model, however, has other hyperparameters controlling path sampling.

Beyond SPAGAN, Chen et al. (2019) concatenate node features, edge features, distances, and ring flags to compute attention probabilities. Li et al. (2020) show that distance encodings (i.e., one-hot feature of distance as an extra node attribute) obtain more expressive power than the 1-Weisfeiler-Lehman test. Graph-BERT introduces multiple positional encodings to apply Transformers to graphs and operates on sampled subgraphs to handle large graphs (Zhang et al., 2020). Yang et al. (2019) introduce the Graph Transformer Network (GTN) for learning a new graph structure, which identifies “meta-paths” and multi-hop connections to learn node representations. Wang et al. (2021a) introduce Multi-hop Attention Graph Neural Network (MAGNA) that uses diffusion to extend attention to multi-hop connections. Frankel et al. (2021) extend GAT attention to a stochastically-sampled neighborhood of neighbors within 5-hops of the central node. Isufi et al. (2020) introduce EdgeNets, which allow for flexible multi-hop diffusion.

Each layer of our GNN attends to the r -ring around each node. Unlike SPAGAN and Graph-BERT, we do not perform sampling, avoiding their sampling-ratio and number-of-iterations hyperparameters. Unlike GTN, we do not restrict to a particular graph structure. Broadly, our approach does not require architecture or optimization changes.

Our work also joins a trend of decoupling the input graph from the graph used for information propagation. For scalability, Hamilton et al. (2017) sample from a node’s

local neighborhood to generate embeddings and aggregate features, while Zhang et al. (2018) sample to deal with topological noise. Rossi et al. (2020) introduce Scalable Inception Graph Neural Networks (SIGN), which avoid sampling by precomputing convolutional filters. Kipf and Welling (2017) preprocess diffusion on graphs for efficient training. Topping et al. (2021) use graph curvature to rewire graphs and combat over-squashing and bottlenecks.

In contrast, our work does not use diffusion, curvature, or sampling, but expands receptive fields via Transformer-inspired positional encodings. In this sense, we avoid the inductive biases from pre-defined notions of diffusion and curvature, and since we do not remove connectivity, injective non-invasive changes are easy to obtain.

3. Preliminaries and Design

Let $G = (V, E, f_v, f_e)$ denote a graph with nodes $V \subset \mathbb{N}_0$ and edges $E \subseteq V \times V$, and let \mathcal{G} be the set of all finite graphs. For each graph, let functions $f_v : V \rightarrow \mathbb{R}^{d_v}$ and $f_e : E \rightarrow \mathbb{R}^{d_e}$ denote node and edge features, respectively. We consider learning on graphs, specially node classification and graph classification.

At inference, the input is a graph G . For node classification, the task is to predict a node label $l_v(v) \in \mathbb{R}$ for each vertex $v \in V$. For graph classification, the task is to predict a label $l_G \in \mathbb{R}$ for the entire graph G .

Given the tasks above, GNN architectures typically ingest a graph $G = (V, E, f_v, f_e)$ and output either a label or a per-node feature. One can view these as an abstraction; e.g. a GNN for graph classification is a map $F_\theta : \mathcal{G} \rightarrow \mathbb{R}^n$ with learnable parameters θ . These architectures vary in terms of how they implement F_θ . Some key examples include

- Spatial models (Kipf and Welling, 2017) use the graph directly, computing new node representations in each layer by aggregating the representations of a node and its neighbors (1-ring).
- Spectral models (Bruna et al., 2014) use the eigendecomposition of the graph Laplacian to perform spectral convolution.
- Diffusion models (Wang et al., 2021a; Klicpera et al., 2019) use weighted sums of powers of the adjacency matrix to incorporate larger neighborhoods.
- In Transformers (Kreuzer et al., 2021; Dwivedi and Bresson, 2021; Rong et al., 2020; Ying et al., 2021), each node forms a new representation by self-attention over the complete graph using positional encodings.

All these approaches aim to incorporate useful inductive biases while remaining flexible enough to learn from data.

Spatial models have been extremely successful, but recent work shows that they struggle with under-reaching and over-squashing (Alon and Yahav, 2021). Spectral approaches have a similar convolutional bias as spatial models but have proved harder to generalize. Transformers with complete attention and diffusion have promising results. Transformers carry little inductive bias but are computationally expensive due to complete attention. Diffusion incorporates the inductive bias that distant nodes should be weighted less in message aggregation.

We aim to alleviate under-reaching and over-squashing while avoiding the computational load of complete attention by incorporating a more general proximity bias than diffusion without committing to a specific model. As with some past works (Hamilton et al., 2017; Zhang et al., 2018; Rossi et al., 2020; Kipf and Welling, 2017; Topping et al., 2021), our method is built on the observation that F_θ can be trained to ingest modified versions of the original graph that better communicate structure and connectivity. Hence, we add new edges, nodes, and features to the input graph. To still convey the original topology of the input graph, we add positional encodings. More formally, we design functions $g : \mathcal{G} \rightarrow \mathcal{G}$ that modify graphs and give features to the new nodes and edges. These functions can be prepended to any GGN $F_\theta : \mathcal{G} \rightarrow \mathbb{R}^n$ as $F_\theta \circ g : \mathcal{G} \rightarrow \mathbb{R}^n$.

The following are desiderata informing our design of g :

- ability to capture the original graph,
- ability to incorporate long-range connections,
- computational efficiency, and
- minimal inductive bias.

By using positional encodings and maintaining the original graph G as a subgraph of the modified graph, we can capture the original graph in our modified input (see Section 4.2.1). By expanding the receptive field around each node to r -rings we reduce computational load relative to complete-graph attention, with limited inductive bias stemming from proximity. Additionally, expanded receptive fields can be shown to alleviate under-reaching and over-squashing; see Section 6.6 for discussion.

4. Approach

Similar to past graph rewiring methods (Hamilton et al., 2017; Zhang et al., 2018; Rossi et al., 2020; Kipf and Welling, 2017; Topping et al., 2021), we modify graphs before using them as input for a downstream GNN model, rather than modifying the model itself. Our approach does not remove any edges or nodes in the original graph but rather only adds elements.

Given an input $G = (V, E, f_v, f_e)$, we create a new graph $G' = (V', E', f'_v, f'_e)$ such that G is a subgraph of G' . Ex-

panded receptive fields are achieved in G' by adding edges decorated with positional encodings as node or edge attributes; we also add a fully-connected CLS node. G' is still a graph with node and edge attributes to which we may apply any GNN. This process is represented by a function $g : \mathcal{G} \rightarrow \mathcal{G}$. We decompose the construction of g into topological rewiring and positional encoding, detailed below.

In a slight abuse of notation, we will subsequently use \mathcal{G} to denote only the subset of graphs relevant to a given machine learning problem. For example, for graph regression on molecules, \mathcal{G} will denote molecule graphs, with atoms as nodes and bonds as edges.

4.1. Topological Rewiring

We modify the input graph G to generate G' in two steps: expanding the receptive field and adding a CLS node.

Expanded receptive field. Given a graph $G = (V, E, f_v, f_e) \in \mathcal{G}$ and a positive integer $r \in \mathbb{N}_+$, we add edges between all nodes within r hops of each other in G to create $G'_r = (V', E', f'_v, f'_e)$. If G is annotated with edge features, we assign to each edge in $E' \setminus E$ an appropriate constant feature C_e .

CLS node. Following Gilmer et al. (2017), we also include a ‘‘CLS’’—or classification—node to our graph connected to all others. Given a graph G , to add a CLS node we initialize with $G' = (V', E', f'_v, f'_e) = G$, add a new node v_{CLS} to V' , and set $f'_v(v_{\text{CLS}}) := C_v$ for a constant C_v . We set $E' := E \cup \bigcup_{v \in V} \{(v_{\text{CLS}}, v), (v, v_{\text{CLS}})\}$, with $f'_e((v_{\text{CLS}}, v)) = f'_e((v, v_{\text{CLS}})) := C_e$, where C_e is defined above.

4.2. Positional Encodings

Given only the connectivity of a rewired graph $G'_r = (V', E', f'_v, f'_e)$ from the two-step procedure above, it may not be possible to recover the connectivity of the original graph $G = (V, E, f_v, f_e)$. In the extreme, when r is large and G is connected, G'_r could become fully-connected, meaning that all topology is lost—removing the central cue for graph-based learning.

To combat the situation above, we encode the original topology of G into G'_r via *positional encodings*, which are node and/or edge features. We consider several positional encoding functions for edges $p_e : \mathcal{G} \times V' \times V' \rightarrow \mathbb{R}^n$ or nodes $p_v : \mathcal{G} \times V' \rightarrow \mathbb{R}^n$, appending the output of p_e as edge or p_v as node features to G'_r .

The approach of adding positional encodings to graphs is inspired by top-performing methods in natural language processing (NLP). In NLP, each input is a piece of text, and positional encodings are used to indicate word order. Positional encodings on graphs via shortest path computa-

tion (see Section 4.2.2) directly adapt this technique from line graphs to more general structures. Our parameter r can then be understood as the maximum sentence length hyperparameter, common in Transformer models such as BERT (Devlin et al., 2018). Unlike NLP, however, there can be multiple nodes with the same positional encoding using the simple shortest-path encoding above, motivating alternative constructions.

Section 4.2.1 lays out distinguishing properties to compare choices of p_e and/or p_v . Then, Section 4.2.2 provides concrete positional encodings compared in our experiments that trade off between the various properties we lay out.

4.2.1. PROPERTIES OF POSITIONAL ENCODINGS

There are countless ways to encode the subgraph topology of G within G' in vertex features p_v or edge features p_e . Below, we state a few properties we can check to give a framework for comparing the capabilities and biases of possible choices.

Lossless encoding. While it is always possible for the GNN that inputs G' to ignore information, it cannot reconstruct information that has been lost in constructing G' from G . On the other hand, there can be benefits in forgetting information, e.g. when dealing with noisy graphs or when incorporating a stronger inductive bias (Rossi et al., 2020; Klicpera et al., 2019). That said, a simple property to check for G' equipped with positional encoding features p_e, p_v is whether we can recover G from this information, that is, whether our encoding is *lossless* (or *non-invasive*).

As long as it is possible to identify G within $g(G)$, g is an injection and non-invasive. Hence, a sufficient condition for lossless positional encodings is as follows: If all 1-hop edges in G' have unique positional encodings, then $g: \mathcal{G} \rightarrow \mathcal{G}$ is a bijection. One way to achieve this condition is to use an additional edge feature that is unique to the 1-ring.

Discriminative power. Following work investigating the discriminative power of GNNs (Xu et al., 2019; Brüel Gabrielsson, 2020), Ying et al. (2021) showed that expanded receptive fields together with shortest-path positional encodings are strictly more powerful than the 1-Weisfeiler-Lehman (WL) test and hence more powerful than 1-ring vanilla spatial GNN models (Xu et al., 2019). The combination of increased receptive fields, positional encodings, and choice of subsequent GNN models determines discriminative power. In fact, it follows from (Ying et al., 2021) that the positional encodings presented below together with an increased receptive field $r > 1$ and a vanilla spatial GNN model are strictly more powerful than the 1-WL test.

Computational time. Although shortest-path distances come for free in our construction of G'_r from G , other more

complicated—but more informative—positional encodings come at substantial computational cost per r -ring. The cost of computing positional encodings affects total inference time, which may be relevant in some learning settings.

Local vs. global. The positional encoding of a vertex or edge can be local, meaning it incorporates information from a limited-sized neighborhood in G , or global, in which case adding or removing a node anywhere in G could affect all the positional encodings.

Inductive bias. Our positional encodings can bias the results of the learning procedure, effectively communicating to the downstream GNN which properties of G and G' are particularly important for learning. In the extreme case, if we do not use positional encodings at all, our model would induce a bias stating that distances $< r$ in our graph are insignificant. More subtly, suppose ℓ is the distance (of length $\leq r$) between two nodes in G corresponding to a new edge in E' . Using ℓ directly as a positional encoding rather than a decaying function, e.g. $e^{-\alpha\ell}$, makes it easier or harder (resp.) to distinguish long distances in the graph.

A related consideration involves whether our model can imitate the inductive bias of past work. For example, graph diffusion has been used to incorporate multi-hop connections into GNNs using fixed weights (Wang et al., 2021a). We can ask whether our positional encodings on G' are sufficient to learn to imitate the behavior of a prescribed multi-hop model on G , e.g. whether a layer of our GNN applied to G' can capture multi-hop diffusion along G .

Over-squashing and under-reaching. We show in Section 6.6 that increased receptive fields as well as the CLS-node alleviate the over-squashing problem. We do this via the NeighborsMatch problem (Alon and Yahav, 2021); however, this toy problem is concerned with matching node attributes and is not concerned with graph topology. Future work may explore other over-squashing problems where positional encodings can be evaluated.

4.2.2. POSITIONAL ENCODING OPTIONS

Taking the properties above into consideration, we now give a few options for positional encodings below, compared empirically in Section 6.

Shortest path. For any edge $e \in G'_r$, the *shortest-path positional encoding* takes $p_e \in \{0, 1, \dots, r\}$ to be the integer length of the shortest path in G between the corresponding nodes of E . These embeddings are lossless because G is the subgraph of $g(G)$ with $p_e = 1$. They also are free to compute given our construction of G'_r from G . But, multiple vertices in the r -neighborhood of a vertex in V could have the same positional encoding in V' , and shortest path lengths are insufficient to capture complex inductive biases of multi-hop GNNs like diffusion over large neighborhoods.

Shortest-path positional encoding was previously used by Ying et al. (2021), but they did not consider smaller r values.

Spectral embedding. Laplacian eigenvectors embed graph vertices into Euclidean space, providing per-vertex features that capture multi-scale graph structure. They are defined by factorizing the graph Laplacian matrix

$$\Delta = I - D^{-1/2} A D^{-1/2},$$

where D is the degree matrix and A is the adjacency matrix. We call the result a *spectral positional embedding*.

We can use the ℓ smallest non-trivial Laplacian eigenvectors of G as a node-based positional encoding $p_v : V' \rightarrow \mathbb{R}^\ell$. Following Dwivedi et al. (2020), since these eigenvectors are known only up to a sign, we randomly flip the sign during training. Prior work has considered using Laplacian eigenvectors as additional node features in GNNs without topological rewiring (Dwivedi et al., 2020). Below we discuss the properties of this choice of positional encoding when combined with our rewiring approach.

Spectral positional encodings do not necessarily make g injective. Even when $\ell = |V|$, this encoding fails to distinguish isospectral graphs (Von Collatz and Sinogowitz, 1957), but these are rarely encountered in practice. On the other hand, spectral signatures are common for graph matching and other tasks. Moreover, unlike the remaining features in this section, spectral positional encodings capture global information about G rather than only r -neighborhoods.

The time complexity of spectral embedding is the time to compute eigenvectors of G 's Laplacian matrix, which can be substantial for large and/or dense graphs. While we compute exact eigenvectors in our experiments, future work can consider methods like (Tropp et al., 2017), which provide lower-cost Laplacian eigenvectors approximations that may suffice for our application.

Finally, we note that the diffusion equation for graphs can be written as $u_t = -\Delta u$; this graph PDE can be solved in closed-form given the eigenvectors and eigenvalues of Δ . Hence, given the spectral embedding of G in G' , we can simulate diffusion-based multi-hop GNN architectures up to spectral truncation.

Powers of the adjacency matrix. Our final option for positional encoding generalizes the shortest path encoding and can capture the inductive biases of diffusion-based GNNs.

The entry at position (i, j) of the k -th power A^k of the adjacency matrix A of the graph G gives the number of paths of length k between node i and j in G . Thus, concatenating the powers from $k = 1, \dots, r$, we get for each edge e in G' an integer vector $p_e \in \mathbb{N}^r$ giving the *powers of the adjacency matrix positional encoding*.

Similarly to the distance-based positional encoding, we can recover the original graph G from this encoding using the first entry of p_e , i.e. where it is non-zero. A straightforward argument shows that this embedding also can be used to recover the shortest-path embedding. Its computational expense is somewhere between the previous two options, requiring $\sim \log r$ matrix multiplies to compute the A^r .

Similarly to the spectral embedding, this adjacency-derived embedding can generalize the inductive bias of diffusion-based multi-hops GNNs. In particular, diffusion aggregation weights are often approximated using a Taylor series

$$\mathcal{W} = \sum_{i=0}^{\infty} \theta_i A^i \approx \sum_{i=0}^r \theta_i A^i := W,$$

where θ_i are a prescribed decaying sequence ($\theta_i > \theta_{i+1}$).

The entries of W above can be computed linearly from the adjacency-powers positional encoding. Hence, it is strictly more general than using prescribed diffusion-based aggregation weights on G .

5. Implementation Details

We apply the GatedGCN (Bresson and Laurent, 2018) and an implementation of the Transformer model (Vaswani et al., 2017). For each model, we run with different sizes for the r -ring receptive field around each node, we compare with and without the CLS-node, and we compare the three positional encodings introduced in Section 4.2.2.

Input and readout layers. Typically, GNNs on a graph $G = (V, E, f_v, f_e)$ first embed node features f_v and edge features f_e through a small feed-forward network (FFN) *input layer*. When incorporating positional encodings per edge/node, we embed using a small FFN and add them at this input layer. After this layer, it updates node and edge representations through successive applications of GNN layers.

Lastly, a *readout layer* is applied to the last GNN layer L . For node classification, it is typically a FFN applied to each node feature h_i^L . For graph classification, it is typically an FFN applied to the mean or sum aggregation of all node features h^L . For graph classification and when using the CLS-node, we apply the FFN to the CLS-node's feature in the last layer, instead of mean or sum aggregation.

Transformer. Our Transformer is a simple implementation with multi-head attention, incorporating edge features through addition in the calculation of attention scores; see Appendix B for details.

Table 1. Effect of increasing r -hops on the ratio of number of edges to number of nodes squared (fully-connected), for the datasets and r -values used in experiments. Dashes indicate that experiments were not run with the corresponding r -value and dataset.

dataset:	ZINC	CLUSTER	PATTERN	MNIST	CIFAR10	NeighborsMatch $r_p = 5$
r=1	0.14	0.31	0.43	0.13	0.08	0.031
r=2	0.27	>0.99	>0.99	0.34	0.21	0.047
r=3	0.40	1.0	1.0	0.58	0.38	0.061
r=4	0.52	-	-	-	-	0.073
r=5	0.62	-	-	-	-	-
r=6	0.71	-	-	-	-	-
r=7	0.79	-	-	-	-	-
r=8	0.85	-	-	-	-	-
r=9	0.90	-	-	-	-	-
r=10	0.94	-	-	-	-	-

6. Experiments

We evaluate and compare performance on five benchmark graph datasets: ZINC, PATTERN, CLUSTER, MNIST, and CIFAR10 from (Dwivedi et al., 2020). The benchmark includes a training time limit of 12 hours; we use similar compute to their work via a single TeslaV100 GPU. Training also stops if for a certain number of epochs the validation loss does not improve. Thus, our benchmark tests for ease of training and efficient use of compute. See Appendix A for details.

For the two first datasets, we run both GatedGCN and Transformer to show that rewiring and positional encoding work for different models; for the other datasets we run only with GatedGCN to focus on the effects of receptive field size, the CLS node, and positional encodings. For all datasets, we run with increasing receptive fields, with different positional encodings, and with or without the CLS-node.

The largest performance increases are accomplished with relatively small receptive fields; after the peak, performance degenerates as the receptive field grows. We stop increasing the receptive field if all modified graphs are already fully connected at previous receptive field size, or if such an increase yields out-of-memory errors. See Appendix A for details and Table 1 for a breakdown of how receptive field size affects the sizes of the graphs.

Table 2 compares our best results with other top performing methods and models. All our top performing models come from the GatedGCN, although the Transformer performs comparably when trained and tested on the same data. Our approach with 100K parameters achieves state-of-the-art on all datasets among models with 100K parameters and for all but the ZINC dataset for models with 500K parameters.

Note that GatedGCN performs overall slightly better than the Transformer; the Transformer was also harder to train,

see Appendix B for details. Our GatedGCN implementation was taken from the same work (Dwivedi et al., 2020) that introduced the benchmarks and code that we use. Thus, hyperparameters might be more carefully adapted to the GatedGCN; however, this highlights the benefits of our model-agnostic approach which allows us to take the top-performing GatedGCN from (Dwivedi et al., 2020) and directly apply it to our work.

6.1. ZINC, Graph Regression

ZINC consists of molecular graphs with the task of graph property regression for constrained solubility. Each ZINC molecule is represented as a graph of atoms as nodes and bonds as edges. From Table 1, we can see that these graphs are very sparse and that the number of edges increases almost linearly as the receptive field r is increased.

Results can be found in Table 3 for r -hops from 1 to 10. Not all graphs are fully-connected at $r = 10$, but since the performance is everywhere decreasing, r was not increased further. Performance across all settings improves significantly when increasing r above 1. Top performance is achieved with the CLS-node and powers-of-the-adjacency positional encoding at $r = 4$; this result is achieved, according to Table 1, at 52% of the edges and compute compared to complete attention. When using the CLS node and/or spectral positional encodings, top performance generally occurs at lower r , which could be due to the global nature of these changes. The GatedGCN and Transformer perform comparably for the same settings, with a slight edge to the GatedGCN. The two models show the same performance trends between settings; i.e. that both increased receptive fields as well as the CLS-node boost performance.

6.2. CLUSTER, Node Classification

CLUSTER is a node classification dataset generated using a stochastic block model (SBM). The task is to assign a cluster label to each node. There are total 6 cluster labels.

CLUSTER graphs do not have edge features.

Table 4 gives results for r -hops from 1 to 3. As can be seen in Table 1, at $r = 3$ all graphs are fully connected, and more than 99% of them are fully connected at $r = 2$. Hence, these graphs are very dense. Significant improvements are achieved by increasing r for all but the spectral positional encoding, which together with the CLS node performs competitively at $r = 1$. The CLS node is helpful overall, especially at $r = 1$. The GatedGCN and Transformer models perform comparably for all but the spectral positional encoding where the Transformer model breaks down. We found that this breakdown was due to the placement of batch normalization, discussed in Appendix B.1.

6.3. PATTERN, Node Classification

Like CLUSTER, the PATTERN dataset is also generated using a SBM model. The task is to classify the nodes into two communities. These graphs do not have edge features.

Table 5 shows results for r -hops from 1 to 3. Similarly to CLUSTER, Table 1 shows that the graphs are very dense. Significant improvements are achieved by increasing $r > 1$ and/or using the CLS-node. Performance generally decreases at $r = 3$. Similarly to CLUSTER, the CLS-node always helps at $r = 1$, but for both CLUSTER and PATTERN, the top performing model comes from a larger $r > 1$ without the CLS-node, suggesting that trade-offs exist between CLS-node and increased receptive fields.

6.4. MNIST, Graph Classification

MNIST is an image classification dataset converted into super-pixel graphs, where each node's feature includes super-pixel coordinates and intensity. The images are of handwritten digits, and the task is to classify the digit.

Table 6 gives results for r -hops from 1 to 3. Not all graphs are fully connected at $r = 3$, but training at $r = 4$ exceeds our memory limit. Significant improvement gains are achieved at $r = 2$, but performance generally decreases at $r = 3$. Also, there is no clear overall positive or negative impact of the use of the CLS-node.

6.5. CIFAR10, Graph Classification

Like MNIST, CIFAR10 is an image classification dataset converted into graphs using super-pixels and assigning each node's features as the super-pixel coordinates and intensity. The images consists of ten natural motifs, and the task is to classify the correct motif, e.g., dog, ship, or airplane.

Table 7 provides results for r -hops from 1 to 3. Not all graphs are fully connected at $r = 3$, but training at $r = 4$ led to out-of-memory issues. Top performing versions are all

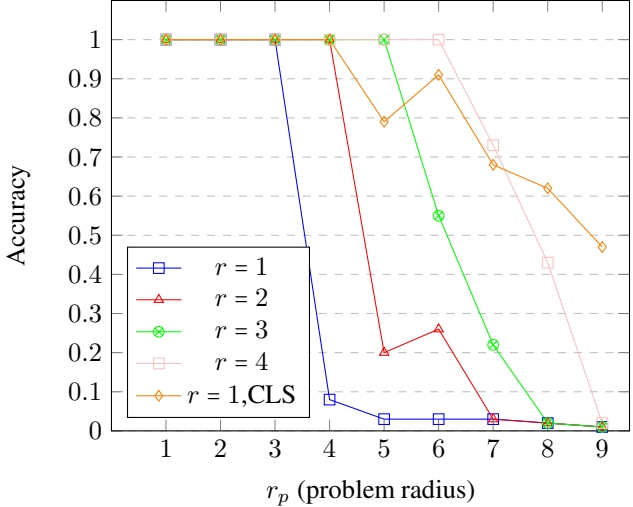


Figure 1. NeighborsMatch (Alon and Yahav, 2021). Benchmarking the extent of over-squashing via the problem radius r_p .

at $r = 1$, and performance degrades for $r > 1$. For $r = 1$, the use of the CLS-node consistently boosts performance, while for $r = 3$ it consistently reduces performance, though very slightly.

6.6. NeighborsMatch, Over-squashing

Alon and Yahav (2021) introduce a toy problem called *NeighborsMatch* to benchmark a GNN's extent of over-squashing, while controlling over-squashing by limiting the problem radius r_p . The graphs in the dataset are binary trees of depth equal to the problem radius r_p . Thus, the graphs are highly structured and sparse, and the number of edges does not grow exponentially with the increased receptive field r , but rather linearly; see Table 1 for an example with problem radius $r_p = 5$. See Figure 1 for results with GatedGCN.

Increasing the receptive field r with a step of 1 increases the problem radius with a step of 1, while using the CLS-node at $r = 1$ falls in between the performance of $r = 2$ and $r = 3$ but with a much longer tail. Thus, this further showcases the difference in effect (complementary as well as conflicting) the receptive field and the CLS-node may have, as also seen on the other benchmarks.

7. Discussion

As verified in experiments across settings, models, and benchmarks, our graph rewiring and positional encodings achieve state-of-the-art GNN performance, widening receptive fields while alleviating over-squashing as demonstrated in the NeighborsMatch experiment.

In our experience, the GatedGCN model was less sensitive to hyperparameters than the Transformer model. This observation highlights the benefits of our model-agnostic ap-

Table 2. Benchmarking. Higher is better for all but for ZINC where lower is better. All results can be found in (Dwivedi et al., 2020; Corso et al., 2020; Bouritsas et al., 2020) and the leaderboard at this [link](#). The benchmarks and corresponding leaderboard have 100K and 500K parameter entries, with many models only appearing with a subset of datasets or number of parameters; dashes indicate that the result for corresponding model, number of parameters, and dataset was not found in their paper or on the leaderboard.

Datasets:	PATTERN	CLUSTER	MNIST	CIFAR10	ZINC
task:	node class.	node class.	graph class.	graph class.	graph reg.
# graphs:	14000	12000	70000	60000	12000
Avg # nodes:	117.47	117.20	70.57	117.63	23.16
Avg # edges:	4749.15	4301.72	564.53	941.07	49.83
MoNet(100K)	85.482±0.037	58.064±0.131	90.805±0.032	54.655±0.518	0.397±0.010
GAT(100K)	75.824±1.823	57.732±0.323	95.535±0.205	64.223±0.455	0.475±0.007
PNA(100K)	-	-	97.940±0.120	70.350±0.630	0.188±0.004
PNA(500K)	-	-	-	-	0.142±0.010
DGN(100K)	-	-	-	72.838±0.417	-
GSN(100K)	-	-	-	-	0.140±0.006
GSN(500K)	-	-	-	-	0.101±0.010
GatedGCN(100K)	84.480±0.122	60.404±0.419	97.340±0.143	67.312±0.311	0.328±0.003
GatedGCN-PE/E(500K)	86.363±0.127	74.088±0.344	-	-	0.214±0.006
Ours (100K)	86.757±0.031	77.575±0.149	98.743±0.062	73.808±0.193	0.143±0.006

Table 3. Increasing r -hops on ZINC/molecules 100K parameters.

type:	trans-adj	trans-adj-cls	trans-short	trans-short-cls	trans-lp	trans-lp-cls	gcn-adj	gcn-adj-cls	gcn-short	gcn-short-cls	gcn-lp	gcn-lp-cls
r=1	0.341±0.024	0.289±0.012	0.346±0.022	0.298±0.012	0.293±0.044	0.257±0.036	0.329±0.023	0.287±0.010	0.326±0.024	0.265±0.043	0.291±0.029	0.274±0.027
r=2	0.297±0.019	0.234±0.021	0.295±0.030	0.220±0.040	0.263±0.024	0.253±0.030	0.265±0.021	0.198±0.011	0.263±0.019	0.204±0.022	0.233±0.023	0.199±0.009
r=3	0.233±0.010	0.150±0.003	0.287±0.024	0.197±0.014	0.297±0.018	0.243±0.019	0.199±0.007	0.152±0.007	0.243±0.005	0.153±0.005	0.254±0.006	0.214±0.007
r=4	0.217±0.014	0.145±0.003	0.294±0.027	0.194±0.014	0.325±0.013	0.288±0.032	0.180±0.009	0.143±0.006	0.236±0.008	0.167±0.010	0.305±0.010	0.307±0.028
r=5	0.226±0.022	0.146±0.006	0.303±0.012	0.200±0.019	0.349±0.006	0.331±0.019	0.165±0.010	0.144±0.005	0.254±0.015	0.175±0.006	0.331±0.013	0.297±0.023
r=6	0.206±0.005	0.169±0.010	0.305±0.014	0.209±0.016	0.373±0.012	0.343±0.009	0.171±0.007	0.152±0.007	0.255±0.009	0.185±0.009	0.352±0.005	0.337±0.009
r=7	0.206±0.013	0.165±0.008	0.318±0.012	0.211±0.017	0.371±0.017	0.336±0.003	0.172±0.007	0.152±0.004	0.259±0.013	0.197±0.004	0.351±0.005	0.327±0.012
r=8	0.212±0.012	0.180±0.010	0.341±0.035	0.235±0.031	0.369±0.009	0.338±0.009	0.192±0.008	0.182±0.012	0.276±0.019	0.210±0.025	0.345±0.006	0.330±0.006
r=9	0.216±0.007	0.203±0.022	0.385±0.013	0.225±0.009	0.396±0.008	0.342±0.007	0.214±0.012	0.257±0.017	0.280±0.020	0.205±0.011	0.363±0.017	0.332±0.011
r=10	0.247±0.021	0.238±0.014	0.366±0.027	0.245±0.023	0.398±0.009	0.350±0.011	0.270±0.045	0.304±0.032	0.275±0.008	0.206±0.010	0.370±0.013	0.336±0.003

gcn: GatedGCN, trans: Transformer, adj: adjacency p.e., short: shortest-path p.e., lp: spectral p.e., cls: CLS-node

Table 4. Increasing r -hops on CLUSTER 100K parameters. *: Means training was unstable and loss did not converge.

type:	trans-adj	trans-adj-cls	trans-short	trans-short-cls	trans-lp*	trans-lp-cls*	gcn-adj	gcn-adj-cls	gcn-short	gcn-short-cls	gcn-lp	gcn-lp-cls
r=1	73.124±0.264	73.972±0.123	73.346±0.119	74.117±0.363	53.858±7.832	48.950±0.887	72.492±0.460	73.459±0.197	72.554±0.418	73.048±0.220	76.453±0.105	77.156±0.181
r=2	76.964±0.059	77.193±0.072	76.498±0.216	76.432±0.115	47.140±11.138	53.381±4.887	76.917±0.059	76.874±0.172	75.354±0.115	75.411±0.063	77.445±0.153	77.520±0.176
r=3	77.095±0.250	77.266±0.133	76.364±0.085	76.636±0.049	37.274±14.859	54.194±1.746	61.028±2.334	61.540±2.404	75.255±0.199	75.392±0.190	77.575±0.149	77.560±0.195

gcn: GatedGCN, trans: Transformer, adj: adjacency p.e., short: shortest-path p.e., lp: spectral p.e., cls: CLS-node

Table 5. Increasing r -hops on PATTERN 100K parameters.

type:	gcn-adj	gcn-adj-cls	gcn-short	gcn-short-cls	gcn-lp	gcn-lp-cls
r=1	85.715±0.036	86.723±0.006	85.681±0.033	86.732±0.020	86.547±0.026	86.713±0.031
r=2	86.698±0.047	86.707±0.029	86.757±0.031	86.736±0.014	86.723±0.031	86.747±0.011
r=3	85.471±0.949	84.657±0.977	86.712±0.031	86.739±0.027	86.718±0.024	86.744±0.015

gcn: GatedGCN, adj: adjacency p.e., short: shortest-path p.e., lp: spectral p.e., cls: CLS-node

Table 6. Increasing r -hops on MNIST 100K parameters.

type:	gcn-adj	gcn-adj-cls	gcn-short	gcn-short-cls	gcn-lp	gcn-lp-cls
r=1	98.537±0.089	98.522±0.033	98.373±0.126	98.545±0.057	98.395±0.099	98.542±0.079
r=2	98.630±0.134	98.743±0.062	98.597±0.070	98.552±0.107	98.720±0.067	98.605±0.032
r=3	98.035±0.094	98.190±0.141	98.315±0.156	98.390±0.104	98.513±0.145	98.570±0.117

gcn: GatedGCN, adj: adjacency p.e., short: shortest-path p.e., lp: spectral p.e., cls: CLS-node

Table 7. Increasing r -hops on CIFAR10 100K parameters.

type:	gcn-adj	gcn-adj-cls	gcn-short	gcn-short-cls	gcn-lp	gcn-lp-cls
r=1	73.415±0.717	73.498±0.842	72.610±0.574	72.950±0.520	72.525±0.471	73.808±0.193
r=2	72.037±0.400	72.480±0.420	72.127±0.471	71.470±0.508	72.085±0.487	71.745±0.325
r=3	70.688±0.171	69.580±0.488	71.285±0.722	71.188±0.498	70.380±0.308	70.318±0.295

gcn: GatedGCN, adj: adjacency p.e., short: shortest-path p.e., lp: spectral p.e., cls: CLS-node

proach, since the GatedGCN implementation stems from a larger body of work on GNNs applied to graphs. Hence, we can reap the benefits of such work without foregoing benefits associated with the Transformer model, whose introduction to graph learning is still relatively recent.

Future work may combine multiple positional encodings, increase number of model parameters, or use more sophisticated features for new edges, like weighted combinations of edge features along the paths. We can also attempt to design an automatic procedure for finding an optimal r for a given problem, balancing compute and performance.

Acknowledgements

The MIT Geometric Data Processing group acknowledges the generous support of Army Research Office grants W911NF2010168 and W911NF2110293, of Air Force Office of Scientific Research award FA9550-19-1-031, of National Science Foundation grants IIS-1838071 and CHS-1955697, from the CSAIL Systems that Learn program, from the MIT-IBM Watson AI Laboratory, from the Toyota-CSAIL Joint Research Center, from a gift from Adobe Systems, and from the Skoltech-MIT Next Generation Program.

References

U. Alon and E. Yahav. On the bottleneck of graph neural networks and its practical implications. In *International Conference on Learning Representations*, 2021.

J. Baek, M. Kang, and S. J. Hwang. Accurate learning of graph representations with graph multiset pooling, 2021.

P. Barceló, E. V. Kostylev, M. Monet, J. Pérez, J. Reutter, and J. P. Silva. The logical expressiveness of graph neural networks. In *International Conference on Learning Representations*, 2020.

G. Bouritsas, F. Frasca, S. Zafeiriou, and M. M. Bronstein. Improving graph neural network expressivity via subgraph isomorphism counting. *CoRR*, abs/2006.09252, 2020.

X. Bresson and T. Laurent. Residual gated graph convnets, 2018.

R. Brüel Gabrielsson. Universal function approximation on graphs. In H. Larochelle, M. Ranzato, R. Hadsell, M. F. Balcan, and H. Lin, editors, *Advances in Neural Information Processing Systems*, volume 33, pages 19762–19772. Curran Associates, Inc., 2020.

J. Bruna, W. Zaremba, A. Szlam, and Y. LeCun. Spectral networks and locally connected networks on graphs. In Y. Bengio and Y. LeCun, editors, *2nd International Conference on Learning Representations, ICLR 2014, Banff, AB, Canada, April 14-16, 2014, Conference Track Proceedings*, 2014.

D. Cai and W. Lam. Graph transformer for graph-to-sequence learning. *CoRR*, abs/1911.07470, 2019.

B. Chen, R. Barzilay, and T. Jaakkola. Path-augmented graph transformer network, 2019.

G. Corso, L. Cavalleri, D. Beaini, P. Liò, and P. Veličković. Principal neighbourhood aggregation for graph nets. In *Advances in Neural Information Processing Systems*, 2020.

Z. Dai, Z. Yang, Y. Yang, J. G. Carbonell, Q. V. Le, and R. Salakhutdinov. Transformer-xl: Attentive language models beyond a fixed-length context. *CoRR*, abs/1901.02860, 2019.

J. Devlin, M.-W. Chang, K. Lee, and K. Toutanova. Bert: Pre-training of deep bidirectional transformers for language understanding. *arXiv preprint arXiv:1810.04805*, 2018.

V. P. Dwivedi and X. Bresson. A generalization of transformer networks to graphs, 2021.

V. P. Dwivedi, C. K. Joshi, T. Laurent, Y. Bengio, and X. Bresson. Benchmarking graph neural networks, 2020.

A. Frankel, C. Safta, C. Alleman, and R. Jones. Mesh-based graph convolutional neural networks for modeling materials with microstructure, 2021.

J. Gilmer, S. S. Schoenholz, P. F. Riley, O. Vinyals, and G. E. Dahl. Neural message passing for quantum chemistry. In *Proceedings of the 34th International Conference on Machine Learning - Volume 70*, ICML’17, page 1263–1272. JMLR.org, 2017.

W. Hamilton, Z. Ying, and J. Leskovec. Inductive representation learning on large graphs. In I. Guyon, U. V. Luxburg, S. Bengio, H. Wallach, R. Fergus, S. Vishwanathan, and R. Garnett, editors, *Advances in Neural Information Processing Systems*, volume 30. Curran Associates, Inc., 2017.

Z. Hu, Y. Dong, K. Wang, and Y. Sun. Heterogeneous graph transformer. *CoRR*, abs/2003.01332, 2020.

E. Isufi, F. Gama, and A. Ribeiro. Edgenets: Edge varying graph neural networks. *CoRR*, abs/2001.07620, 2020.

G. Ke, D. He, and T. Liu. Rethinking positional encoding in language pre-training. *CoRR*, abs/2006.15595, 2020.

D. P. Kingma and J. Ba. Adam: A method for stochastic optimization. In Y. Bengio and Y. LeCun, editors, *3rd International Conference on Learning Representations, ICLR 2015, San Diego, CA, USA, May 7-9, 2015, Conference Track Proceedings*, 2015.

T. N. Kipf and M. Welling. Semi-supervised classification with graph convolutional networks. In *5th International Conference on Learning Representations, ICLR 2017, Toulon, France, April 24-26, 2017, Conference Track Proceedings*. OpenReview.net, 2017.

J. Klicpera, S. Weißenberger, and S. Günnemann. *Diffusion Improves Graph Learning*. Curran Associates Inc., Red Hook, NY, USA, 2019.

D. Kreuzer, D. Beaini, W. L. Hamilton, V. Léturneau, and P. Tossou. Rethinking graph transformers with spectral attention. *CoRR*, abs/2106.03893, 2021.

P. Li, Y. Wang, H. Wang, and J. Leskovec. Distance encoding: Design provably more powerful neural networks for graph representation learning, 2020.

N. Parmar, A. Vaswani, J. Uszkoreit, L. Kaiser, N. Shazeer, A. Ku, and D. Tran. Image transformer. In J. Dy and A. Krause, editors, *Proceedings of the 35th International Conference on Machine Learning*, volume 80 of *Proceedings of Machine Learning Research*, pages 4055–4064. PMLR, 10–15 Jul 2018.

Y. Rong, Y. Bian, T. Xu, W. Xie, Y. WEI, W. Huang, and J. Huang. Self-supervised graph transformer on large-scale molecular data. In H. Larochelle, M. Ranzato, R. Hadsell, M. F. Balcan, and H. Lin, editors, *Advances in Neural Information Processing Systems*, volume 33, pages 12559–12571. Curran Associates, Inc., 2020.

E. Rossi, F. Frasca, B. Chamberlain, D. Eynard, M. M. Bronstein, and F. Monti. Sign: Scalable inception graph neural networks. *CoRR*, abs/2004.11198, 2020.

Y. Shi, Z. Huang, S. Feng, H. Zhong, W. Wang, and Y. Sun. Masked label prediction: Unified message passing model for semi-supervised classification, 2021.

J. Topping, F. Di Giovanni, B. P. Chamberlain, X. Dong, and M. M. Bronstein. Understanding over-squashing and bottlenecks on graphs via curvature. *arXiv preprint arXiv:2111.14522*, 2021.

J. A. Tropp, A. Yurtsever, M. Udell, and V. Cevher. Fixed-rank approximation of a positive-semidefinite matrix from streaming data. In *Advances in Neural Information Processing Systems*, volume 30, 2017.

A. Vaswani, N. Shazeer, N. Parmar, J. Uszkoreit, L. Jones, A. N. Gomez, L. u. Kaiser, and I. Polosukhin. Attention is all you need. In I. Guyon, U. V. Luxburg, S. Bengio, H. Wallach, R. Fergus, S. Vishwanathan, and R. Garnett, editors, *Advances in Neural Information Processing Systems*, volume 30. Curran Associates, Inc., 2017.

P. Veličković, G. Cucurull, A. Casanova, A. Romero, P. Liò, and Y. Bengio. Graph attention networks, 2018.

L. Von Collatz and U. Sinogowitz. Spektren endlicher grafen. In *Abhandlungen aus dem Mathematischen Seminar der Universität Hamburg*, volume 21, pages 63–77. Springer, 1957.

G. Wang, R. Ying, J. Huang, and J. Leskovec. Multi-hop attention graph neural networks. In *Proceedings of the Thirtieth International Joint Conference on Artificial Intelligence (IJCAI)*, pages 3089–3096, 2021a.

G. Wang, R. Ying, J. Huang, and J. Leskovec. Multi-hop attention graph neural network, 2021b.

K. Xu, W. Hu, J. Leskovec, and S. Jegelka. How powerful are graph neural networks? In *International Conference on Learning Representations*, 2019.

Y. Yang, X. Wang, M. Song, J. Yuan, and D. Tao. Spagan: Shortest path graph attention network. In *Proceedings of the Twenty-Eighth International Joint Conference on Artificial Intelligence, IJCAI-19*, pages 4099–4105. International Joint Conferences on Artificial Intelligence Organization, 7 2019. doi: 10.24963/ijcai.2019/569.

C. Ying, T. Cai, S. Luo, S. Zheng, G. Ke, D. He, Y. Shen, and T. Liu. Do transformers really perform bad for graph representation? *CoRR*, abs/2106.05234, 2021.

S. Yun, M. Jeong, R. Kim, J. Kang, and H. J. Kim. Graph transformer networks. In H. Wallach, H. Larochelle, A. Beygelzimer, F. d’Alché-Buc, E. Fox, and R. Garnett, editors, *Advances in Neural Information Processing Systems*, volume 32. Curran Associates, Inc., 2019.

M. Zaheer, G. Guruganesh, K. A. Dubey, J. Ainslie, C. Alberti, S. Ontanon, P. Pham, A. Ravula, Q. Wang, L. Yang, and A. Ahmed. Big bird: Transformers for longer sequences. In H. Larochelle, M. Ranzato, R. Hadsell, M. F. Balcan, and H. Lin, editors, *Advances in Neural Information Processing Systems*, volume 33, pages 17283–17297. Curran Associates, Inc., 2020.

J. Zhang, H. Zhang, C. Xia, and L. Sun. Graph-bert: Only attention is needed for learning graph representations, 2020.

Y. Zhang, S. Pal, M. Coates, and D. Üstebay. Bayesian graph convolutional neural networks for semi-supervised classification, 2018.

A. Training Details

Both code and training follow [Dwivedi et al. \(2020\)](#) closely, and to a lesser extent ([Dwivedi and Bresson, 2021](#)), which uses the same code base.

Like ([Dwivedi et al., 2020](#)), we use the Adam optimizer ([Kingma and Ba, 2015](#)) with the same learning rate decay strategy. The initial learning rate is set to 10^{-3} and is reduced by half if the validation loss does not improve after a fixed ("lr_schedule_patience") number of epochs, either 5 or 10. Instead of setting a maximum number of epochs, the training is stopped either when the learning rate has reached 10^{-6} or when the computational time reaches 12 hours (6 hours for NeighborsMatch). Experiments are run with 4 different seeds; we report summary statistics from the 4 results.

Below we include training settings for the different datasets.

A.1. ZINC

```
"model": GatedGCN and Transformer,  
"batch_size": 128,  
"lr_schedule_patience": 10,  
"max_time": 12
```

A.2. CLUSTER

```
"model": GatedGCN and Transformer,  
"batch_size": 48 (GatedGCN), 32 or 16 (Transformer),  
"lr_schedule_patience": 5,  
"max_time": 12
```

A.3. PATTERN

```
"model": GatedGCN,  
"batch_size": 48,  
"lr_schedule_patience": 5,  
"max_time": 12
```

A.4. MNIST

```
"model": GatedGCN,  
"batch_size": 128,  
"lr_schedule_patience": 10,  
"max_time": 12
```

A.5. CIFAR10

```
"model": GatedGCN,  
"batch_size": 128,  
"lr_schedule_patience": 10,  
"max_time": 12
```

A.6. NeighborsMatch

```
"model": GatedGCN,  
"batch_size": 256,  
"lr_schedule_patience": 10,  
"max_time": 6
```

B. Transformer Implementation

We implemented a simple version of the Transformer adapted to graphs:

$$\begin{aligned}\hat{h}_i^l &= \text{BN}(h_i^{l-1}) \\ \hat{h}_i^l &= \left\|_{k=1}^H \left(\sum_{j \in \mathcal{N}_i \cup \{i\}} a_{i,j}^{l,k} W_k^l \hat{h}_j^{l-1} \right) + h_i^{l-1} \right\| \\ h_i^l &= \text{FFN}(\text{BN}(\hat{h}_i^l)) + \hat{h}_i^l\end{aligned}$$

with

$$\begin{aligned}\hat{e}_{i,j}^l &= \text{BN}(e_{i,j}^{l-1}) \\ \hat{a}_{i,j}^{l,k} &= ((A_k^l \hat{h}_i^l)^T (B_k^l \hat{h}_j^l) + C_k^l \hat{e}_{i,j}^l) / d \\ a_{i,j}^{l,k} &= \frac{\exp(\hat{a}_{i,j}^{l,k})}{\sum_{j' \in \mathcal{N}_i \cup \{i\}} \exp(\hat{a}_{i,j'}^{l,k})} \\ e_{i,j}^l &= \text{FFN}(\hat{e}_{i,j}^l) + e_{i,j}^{l-1}\end{aligned}$$

Here, h and e are node and edge features (resp.) from the previous layer. $W_k, A, B \in \mathbb{R}^{d/H \times d}$ and $C \in \mathbb{R}^{1 \times d}$ are learnable weight-matrices, H is the number of attention heads, and BN is short for batch normalization. $\|_{k=1}^H$ denote the concatenation of the attention heads.

B.1. Design Choices and Challenges

There are many variations on the Transformer model. Following Ying et al. (2021), we put the normalization before the multi-head attention, which caused instability when training on CLUSTER with Laplacian (spectral) positional encodings. This was fixed by putting the normalization after or using layer normalization instead of batch normalization; however, these changes reduced performance on ZINC. While the GatedGCN worked well with identical architecture parameters across datasets, we found that the Transformer needed more variations to stay competitive on MNIST and CIFAR10; in particular, fewer layers and larger hidden dimensions.

Transformers use multi-head attention which puts number-of-heads dimension vectors on each edge—seen as directed. Hence, the memory load becomes $2 \times |E| \times \text{num_heads}$ (in our experiments, $\text{num_heads} = 6$), which compared for GatedGCN is only $2 \times |E|$. This causes a memory bottleneck for the Transformer that may force one to use a reduced batch size to avoid memory issues.

B.2. Other Variants

We implemented other variants, including more involved Transformers. As in (Vaswani et al., 2017), we ran the path-integers through sine and cosine functions of different frequencies, and inspired by (Dai et al., 2019; Ke et al., 2020) we implemented a more involved incorporation of relative positions in the multi-head attention (see below); however, we found performance to be comparable.

In natural language processing, the input is a sequence (a line graph) $x = (x_1, \dots, x_n)$ of text tokens from a vocabulary set \mathcal{V} , with each token having a one-hot-encoding $f_{\mathcal{V}} : \mathcal{V} \rightarrow [0, 1]^{\mathcal{V}}$. The word embeddings $E \in \mathbb{R}^{n \times d}$ for n tokens are formed as $E = (W_{\text{embed}} f_{\mathcal{V}}(x_i) \mid x_i \in x)$ where $W_{\text{embed}} \in \mathbb{R}^{d \times |\mathcal{V}|}$ is a learnable weight matrix.

The original Transformer model used *absolute positional encodings*. This means that we add the positional encoding to the node embedding at the input layer. Consider a positional encoding function $p_e : \mathbb{N}_0 \rightarrow \mathbb{R}^d$. Then the first input is

$$h^0 = (W_{\text{embed}} f_{\mathcal{V}}(x_i) + p_e(i) \mid i = 1, \dots, n) = E + U$$

where $U = (p_e(i) \mid i = 0, \dots, n) \in \mathbb{R}^{n \times d}$. Typically p_e contains sine and cosine functions of different frequencies:

$$\begin{aligned}p_e(k, 2 \times l) &= \sin(k/10000^{(2 \times l)/d}) \\ p_e(k, 2 \times l + 1) &= \cos(k/10000^{(2 \times l + 1)/d})\end{aligned}$$

Table 8. Increasing r -hops on ZINC/molecules 100K parameters.

type:	trans-adj	trans-short-cls
r=1	0.338±0.020	0.274±0.021
r=2	0.296±0.010	0.179±0.011
r=3	0.260±0.013	0.183±0.018
r=4	0.255±0.009	0.271±0.036
r=5	0.235±0.022	0.227±0.026
r=6	0.226±0.015	0.264±0.042
r=7	0.219±0.012	0.251±0.039
r=8	0.210±0.009	0.278±0.026
r=9	0.213±0.010	0.289±0.042
r=10	0.564±0.221	0.327±0.023

Table 9. Radii on CLUSTER 100K parameters.

type:	trans-adj-cls	trans-adj	trans-short-cls	trans-short
r=1	74.262±0.188	73.445±0.068	74.717±0.308	72.947±0.123
r=2	77.390±0.168	77.399±0.200	76.771±0.012	76.454±0.084
r=3	77.216±0.226	68.384±7.975	76.770±0.094	76.521±0.250

where $k \in \mathbb{N}$ is the position and $l \in \mathbb{N}$ is the dimension. That is, each dimension of the positional encoding corresponds to a sinusoid. The wavelengths form a geometric progression from 2π to $10000 \times 2\pi$. This function was chosen because it was hypothesized that it would allow the model to easily learn to attend by relative positions, since for any fixed offset m , $p_e(k + m)$ is a linear function of $p_e(k)$. It was also hypothesized that it may allow the model to extrapolate to sequence lengths longer than the ones encountered during training.

In many cases, absolute positional encodings have been replaced with *relative fully learnable positional encodings* and *relative partially learnable positional encodings* (Dai et al., 2019). To justify these, consider the first attention layer with absolute positional encodings:

$$A_{i,j}^{abs} = E_{x_i} W_q W_k^T E_{x_j}^T + E_{x_i} W_q W_k^T U_j^T + U_i W_q W_k^T E_{x_j}^T + U_i W_q W_k^T U_j^T$$

For relative (fully and partially) learnable positional encodings we have instead:

$$A_{i,j}^{rel} = E_{x_i} W_q W_{k,E}^T E_{x_j}^T + E_{x_i} W_q W_{k,R}^T R_{i-j}^T + u W_{k,E}^T E_{x_j}^T + v W_{k,R}^T R_{i-j}^T$$

where $u, v \in \mathbb{R}^{1 \times d}$ are learnable weights and $R_{i-j} \in \mathbb{R}^{1 \times d}$ is a relative positional encoding between i and j . Each term has the following intuitive meaning: term (1) represents content-based addressing, term (2) captures a content-dependent positional bias, term (3) governs a global content bias, and (4) encodes a global positional bias.

For relative fully learnable positional encodings, $W_{k,R}^T R_{i-j}^T$ is a learnable weight in $\mathbb{R}^{d \times 1}$ for each $i - j \in \mathbb{N}$, while for relative partially learnable positional encodings $R_{i,j} = p_e(|i - j|)$ where p_e is the sinusoidal function from before.

We implemented both fully and partially learnable positional encodings for the shortest-path positional encodings (integer-valued) and related versions for the other positional encodings (in \mathbb{R}^d). We include results in Tables 8 and 9.